Fabrication and Testing of a Microneedles Sensor Array for *p*-Cresol Detection with Potential Biofuel Applications

Jason C. Harper,[†] Susan M. Brozik,[†] Jeb H. Flemming,[‡] Jaime L. McClain,[†] Ronen Polsky,[†] Dominic Raj,[§] Gregory A. Ten Eyck,[†] David R. Wheeler,[†] and Komandoor E. Achyuthan*[,†,∥]

Sandia National Laboratories, Albuquerque, New Mexico 87185, Life Bioscience, Albuquerque, New Mexico 87185, George Washington University, Washington, D.C. 20052, and Joint BioEnergy Institute, Emeryville, California 94608

ABSTRACT We present a miniaturized high-throughput sensor array that will augment biofuel technology by facilitating in situ biochemical measurements upon micrometer-scale surfaces of leaves, stems, or petals. We used semiconductor processing to photopattern Foturan glass wafers and fabricated gold-plated microscopic electrode needles (ElectroNeedles) that pierced 125-μm-thick surfaces without deformation. The 5 × 5 or 10 × 10 arrays of ElectroNeedles can analyze 25 or 100 samples simultaneously, increasing throughput. Each microneedle in the array can also be individually addressed and selectively functionalized using diazonium electrodeposition, conferring multiplexing capability. Our microfabrication is a simple, inexpensive, and rapid alternative to the time-, cost-, and protocol-intense, deep-reactive-ion-etching Bosch process. We validated the system performance by electrochemically detecting *p*-cresol, a phenolic substrate for laccase, an enzyme that is implicated in lignin degradation and therefore important to biofuels. Our limits of detection (LOD) and quantization (LOQ) for *p*-cresol were 1.8 and 16μM, respectively, rivaling fluorescence detection (LOD and LOQ = 0.4 and 3μM, respectively). ElectroNeedles are multiplexed, high-throughput, chip-based sensor arrays designed for minimally invasive penetration of plant surfaces, enabling in situ and point-of-test analyses of biofuel-related biochemicals.

KEYWORDS: ElectroNeedles • fabrication • diazonium • *p*-cresol • laccase • electrochemistry • fluorescence

INTRODUCTION

The glucose molecules of cellulose can be saccharified into biofuels. However, cellulose is sheathed in a tough, non-carbohydrate, polymeric lignin matrix, making the lignocellulosic biomass recalcitrant to saccarification (1). To tackle this challenge, the U.S. Department of Energy established three Bioenergy Research Centers, one of which is the Joint BioEnergy Institute (JBEI) (2). One of JBEI's goals is the research and development (R&D) of enabling technologies for second-generation biofuels derived from lignocellulose (1). A miniaturized, high-throughput, penetrable, chip-based sensor array will augment the biofuel technology platform by facilitating in situ biochemical measurements upon the micrometer-thick surfaces of plant leaves, stems, or petals.

Advances in semiconductor processing have led to integrated microsensors including the micron-sized microneedles used almost exclusively for drug delivery (3). Microneedle fabrication usually involves a multistep deep-reactive-ion-etching Bosch process (4) that is labor-, capital-, and time-intensive. We describe an easier, semiconductor-based alternate process for fabricating penetrable microneedles targeted toward biofuel sensor applications rather than drug delivery (3). We photopatterned and etched Foturan glass wafers to make 5 × 5 or 10 × 10 arrays of robust hollow microscopic needles that were then filled with gold by electroplating to form the sensing electrodes (i.e., ElectroNeedles). The ElectroNeedles in the array were covalently modified using diazonium surface chemistry (5). Each needle in the array could also be individually addressed through selective electrodeposition in order to enable multiplexed electrochemical measurements (6, 7). Our fabrication yielded a combination of penetrable needles and exposed electrodes conferring point-of-test capabilities to the sensor array for in situ, minimally invasive biochemical analyses of micron-thin, penetrable plant surfaces such as leaves or petals (8, 9).

Laccases oxidize phenolic and non-phenolic substrates while reducing molecular oxygen to water (10). Most lignin-degrading fungi produce laccase under ligninolytic conditions, prompting speculation for a role in lignin degradation (10). We used the ElectroNeedles to electrochemically detect and quantize *p*-cresol (4-methylphenol), a phenolic substrate for *Trametes versicolor* fungal laccase (11). *p*-Cresol also arises from microbial action upon lignin (12), and it might be a redox mediator of laccase-catalyzed lignin degradation (13). Modeling (14) and experimental investigations (15) have revealed that *p*-cresol is a major component of bio-oils derived from lignin pyrolysis. Grafting *p*-cresol onto lignin-based polymers (lignocresols) was proposed as a method for the enzymatic modification of lignophenols for converting

* To whom correspondence should be addressed. Tel: 505-284-8979. Fax: 505-844-1198. E-mail: kachyut@sandia.gov. Present address: Biosensors & Nanomaterials Department, Sandia National Laboratories, P.O. Box 5800, MS 1425, Albuquerque, NM 87185-1425.

Received for review April 16, 2009 and accepted June 22, 2009

[†] Sandia National Laboratories.

[‡] Life Bioscience.

[§] George Washington University.

[∥] Joint BioEnergy Institute.

DOI: 10.1021/am900259u

lignin into industrial chemicals (16). *p*-Cresol mixed with supercritical water was shown to be an effective solvent for enhancing lignin disassembly (17). Finally, *p*-cresol was shown to react with manganese peroxidase compounds I and II from the extensively studied lignin-degrading basidomycete, *Phanerochaete chrysosporium* (18). Our interest in *p*-cresol and fungal laccases is thus a part of JBEI's R&D effort into enabling technologies for second-generation biofuels (1). We validated the ElectroNeedle system performance against our fluorescence assay for *p*-cresol (11).

Most high-throughput screening (HTS) systems employ large, high-power, sophisticated, bench-top equipment that incorporate complex optics, robotics, and liquid handling. Such systems also require management and maintenance (19). Consequently, these systems are not amenable for on-site, in situ screening of genetically engineered plants to monitor biochemical changes targeted toward improving biofuel production (1, 20). An integrated, miniaturized, high-throughput, field-deployable, portable, and penetrable system such as the ElectroNeedles sensor array might facilitate real time, on-site, in situ, and minimally invasive analyses of phytochemicals that are important to biofuel production (1, 2).

MATERIALS AND METHODS

Laccase enzyme from the white rot basidomycetes fungus *T. versicolor*, *p*-cresol, acetonitrile, nitrobenzene diazonium, tetrabutylammonium tetrafluoroborate (Bu_4NBF_4), and citrate buffer, pH 4.5, were purchased from Sigma-Aldrich (St. Louis, MO). Foturan (a lithium−aluminum−potassium silicate glass containing traces of sodium, zinc, antimony, silver, and cerium) was purchased from Mikroglas Chemtech GmbH/Invenios (Mainz, Germany, and Santa Barbara, CA). Carboxylphenyl diazonium was synthesized as described previously (21). All other chemicals were from various commercial sources. All solutions and buffers were prepared with 18 MΩ · cm water obtained from a Barnstead Nanopure water purifier (Boston, MA). White polypropylene 96-well Optiplate microplates were purchased from Perkin-Elmer (Waltham, MA).

Microfabrication. Fabrication of microneedles involved several distinct processing phases using the photopatternable glass Foturan. Briefly, the general process flow for fabrication was to pattern and etch 100 μm diameter via holes through the glass on a 1-mm pitch. The etched holes were filled with gold by means of electroplating. Both faces were polished to remove plating overburden and gave a clean working surface. A backside metallization was applied using standard liftoff techniques that provided the interconnections between the needles and bond pads used in packaging. At this point, a second etch was performed on the front side of the glass to form the protruding needles. The wafers were then diced into 1 cm × 1 cm die and wire-bonded in a custom carrier that has a machined hole to expose the needles (details below).

Theory. Foturan glass contains Ce^{3+} and Ag_2O in its matrix. When exposed to UV light within the absorption band of the metal ion dopants in the glass, Ce^{3+} acts as a sensitizer, absorbing a photon and stripping an electron. The electrons reduce neighboring Ag^+ ions to form colloidal silver atoms (Ag^+ to Ag^0). The Ag^0 colloids agglomerate during the first baking cycle and serve as nucleation centers for Li_2SiO_3 crystal growth during the second annealing step (22). The Li_2SiO_3 crystals have up to 30 times greater wet etch rate in HF than the surrounding unexposed material, giving the selectivity that is required in order to pattern the features into the bulk of the glass (in this case, the vias (Figure 1).

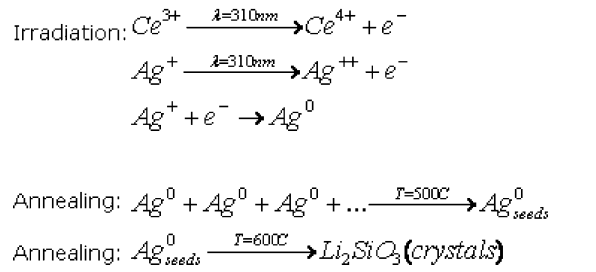

FIGURE 1. General sequence for the exposure and baking of Foturan and the accompanying chemical changes. For additional details, see ref 28.

The degree and type of crystallization (etch rate) are dependent upon the radiation and thermal conditions. The intensity of light reaching a given point (depth) in the glass is based upon both the absorption of the glass itself and the interaction between the photons and Ce^{3+} and Ag^+ ions embedded in the glass. Additional scattering losses also factor into this. The oxidation state of Ag^+ is not changed by thermal treatment, so no additional nuclei are formed during thermal treatment. Silver clusters formed during the early part of the heat treatment are a few hundred atoms in size, and their size does not depend on the temperature but increases with added exposure time (23). Thus, there is a balance between exposure energy and bake conditions for producing uniformly anisotropic features.

Foturan Photopatterning. Wafers were processed using 1.1-mm-thick Foturan, allowing a sufficiently robust glass base to remain after the needle protrusions were formed. Foturan was placed in a mid-UV flood exposure system (ABM, Inc., San Jose, CA) optimized for 310-nm light and exposed through a quartz photomask. The flux was 30 mW/cm^2, and each exposure lasted for 25 min, giving a total dose of 45 J/cm^2. The exposed wafers were baked at 500 °C for 75 min and again at 600 °C for another 75 min, thereby allowing the UV-exposed area to convert to ceramic, creating an image that can be etched later for through-holes. After baking, the exposed regions were dark brown, and the contrast allowed a second mask to be aligned in order to pattern the protruded needles and define the sheath thickness. The negative photoresist protected these areas from UV. The wafers were exposed at 30 mW/cm^2 but for only 15 min in order to expose a desired depth into the Foturan wafer. The shorter exposure allowed the top of the wafer to be etched at a much higher rate than the bottom. The wafers were etched in a 10:1:1 volume ratio of a mixture of a H_2O/HF/HNO_3 solution in an ultrasonic bath for 45 min. This etch created the via holes but did not attack the front surface of the wafer (from second exposure) because the glass was not baked after the second exposure. The final product is hollow microneedles that are 400−500 μm tall with outer and inner diameters of approximately 250 and 100 μm, respectively. We fabricated ElectroNeedles in both hollow microneedle and solid micropost configurations but used only the latter for the electrochemical measurements of *p*-cresol.

Electroplating. The next phase of the processing was the via hole fill with electroplated gold. Successful electroplating requires a seed layer at the bottom of each via that will support a uniform current density across the wafer. A reliable method for this was to metalize the backside of the wafer (200 Å Ti/200 Å Pt/1000 Å Au) and bond it to a support structure that was also coated with the metal. The sandwiched metal layer served as the seed for the electroplating, but because it was only exposed to the bath through the via holes, the plating was confined to the vias. Ideally, a glancing-angle deposition was used for coating of the backside of Foturan to minimize the metal deposition on the sidewalls of the vias. Nonuniform coating on the via sidewalls can lead to gaps in the plated posts. The Foturan wafers have a large bow/warp characteristic (>40 μm)

that is exacerbated by the bake cycle near the glass melting point. Therefore, the wafers must be planarized before bonding them. This is typically accomplished by lapping. Because of difficulties with the lapping facilities, the wafers were not lapped before the backside metal was applied and several bonding strategies were explored to mitigate the risks. One promising strategy was a wafer that was bonded to a sheet of 25-μm-thick titanium foil coated on one side with Ti/Pt/Au. This wafer was then sealed into a plating fixture to avoid backside plating. The bond was successful in some areas, and several die across the wafer were plated.

ElectroNeedle Devices. All of the die except two had solid vias (two plated on the via sidewall but remained hollow metal tubes). Each of these was cleaned by shaving off the plating overburden, hand polishing, and baking at 500 °C for 60 min and then at 600 °C for another 60 min. Liftoff patterning was performed to apply the backside metallization interconnect pattern. These die were then mounted with a crystal bond to a silicon support wafer so that they could be etched to form the needle protrusions. The same glass etch was used (10:1:1 volume ratio of a mixture of H_2O/HF/HNO_3) for 25 min in an ultrasonic bath. These die were further processed into packaged devices (23) for electrochemical measurements of *p*-cresol.

Microscopy. Imaging of the ElectroNeedles and devices was taken using either a Nikon stereooptical microscope with a Nikon coolpix 360 (Nikon Inc., Melville, NY) through the optical lens stereo or a scanning electron microscope. The coolpix 360 is a camera equipped with an angle indicator and an inclinometer to indicate the horizontality of the position. During scanning electron microscopy (SEM), a beam of highly energetic (0.1−50 kV) electrons is focused on a sample surface. Because the electron beam is scanned in the $X-Y$ plane, images can be mapped. The secondary electron detector maps the surface topography down to a resolution of a few nanometers. All scanning electron micrographs were acquired on a JEOL JSM-5800 low-vacuum scanning electron microscope (JEOL USA, Peabody, MA). The microscope is equipped with secondary and backscattered electron detectors as well as a cathodoluminescence detector. The SEM images were taken with a beam voltage of 10 kV and an incident beam current of about 1 μA. The ElectroNeedles were not gold coated prior to imaging with SEM, and some charging does occur on the Foturan glass. The sample was rotated to an angle of about 50° with respect to the incident electron beam to highlight the height and cylindrical shape of the ElectroNeedles (microneedles and microposts).

Electrochemistry. All electrochemical measurements were performed at room temperature (~25 °C) using a PGZ100 Voltalab potentiostat (Radiometer Analytical, Lyon, France) and were measured versus an Ag/AgCl reference (3 M NaCl, aqueous solutions) or Ag/$AgNO_3$ reference (10 mM, nonaqueous solutions, −102 mV versus a ferrocene couple) and a platinum counter electrode from Bioanalytical Systems (West Lafayette, IN). Gold disk electrodes (5 mm diameter) were prepared by thermal evaporation of a 200-Å titanium adhesion layer followed by 2000 Å of gold onto a Pyrex wafer. Gold electrodes were cleaned immediately before use with a freshly prepared "piranha" solution (5:3 volume ratio of H_2SO_4/H_2O_2) for 10 min, then washed with nanopure water, and dried under a stream of N_2.

p-Cresol can be oxidized at potentials between +500 and +800 mV versus Ag/AgCl, allowing for potentiometric electrochemical detection (24). The products of *p*-cresol oxidation are highly reactive phenoxy radicals that polymerize in solution near the electrode surface (24). Cyclic voltammetry (CV) was used to scan from −400 to +900 mV using a scan rate of 100 mV/s. The measurements were performed in a cell using 10 mL of a 50 mM sodium phosphate buffer, pH 7.4, a Ag/AgCl reference electrode, and a platinum wire auxiliary electrode.

Electrode Modification and *p*-Cresol Measurements. Nitrophenyl, carboxy, or aminophenyl thin films were assembled onto clean gold electrodes using two CV scans from 0 to −1 V at 100 mV/s, in a solution of 1 mM nitrophenyl or carboxylphenyl diazonium salt and 0.1 M Bu_4NBF_4 in acetonitrile. After electrodeposition, the electrodes were rinsed with acetonitrile and ethanol followed by 15 s of sonication in ethanol to remove any adsorbed phenyl diazonium. After sonication, the electrodes were rinsed again with ethanol and dried under a stream of N_2. Aminophenyl films were obtained by the six-electron electrochemical reduction of nitrophenyl groups to aminophenyl groups by CV from −300 to −1300 mV in a deoxygenated (argon-sparged) mixture of a 1:9 volume ratio of a mixture of an ethanol/water solution with 0.1 M KCl as the supporting electrolyte. A 50 μL solution of a sodium phosphate buffer containing a particular concentration of *p*-cresol was placed on the array followed by CV at that specific, individually addressable, ElectroNeedle post. Following measurement, the array was thoroughly rinsed and dried before detection of a different *p*-cresol concentration.

Fluorescence Assay of Laccase-Oxidized *p*-Cresol. *p*-Cresol was diluted in a citrate phosphate buffer, pH 4.5, and oxidized using *T. versicolor* fungal laccase in the same buffer at 37 °C for 60 min. Fluorescence from the laccase-catalyzed oxidation products of *p*-cresol was measured after excitation of the samples at either 262 or 322 nm and monitoring of the emission at 425 nm, as described previously (11). Fluorescence measurements were taken using a Molecular Devices M2 model microplate reader (MDS Analytical Technologies, Sunnyvale, CA). Fluorescence intensity is expressed as relative fluorescence units (RFU).

Data Analyses. All data were collected from triplicate measurements. Results were calculated as average ± standard deviation. Where not visible, error bars are masked within the symbol. *Kaleidagraph* (version 4.03, Synergy Software, Reading, PA) was used to create the assay charts using linear or logarithmic curve-fitting options of the software program. Linearity of the dose−response curves was expressed by the correlation coefficient, r^2. The limit of detection (LOD) represents the lowest concentration of an analyte in a positive control reaction whose signal strength is greater than the sum of the signal from the negative control reaction and its standard deviation value multiplied by a factor of 3 (LOD = $\mu + 3\sigma$, where μ equals the mean background signal and σ its standard deviation). The limit of quantitation/quantization (LOQ) is defined as the lowest concentration of an analyte in a positive control reaction that elicits a signal response that is 3 times larger than the LOD signal strength. It should be noted that the LOQ concentration of the analyte is not necessarily 3 times greater than the LOD concentration because these values are related to the signal strength.

RESULTS AND DISCUSSION

A majority of the scientific literature on microneedles is focused on the evaluation of their use in drug-delivery applications (3). Others have described only the fabrication of the needles without providing exemplars of biochemical applications (25, 26), including those claiming lab-on-chip applications (27). Clearly, microneedles as a high-throughput, sensor array for biochemical analyses is in its nascent stage. Most HTSs are done using bench-top, specialized equipment, incorporating sophisticated optics, robotics, and liquid handling that require management and maintenance (19). Such systems are not amenable for the in situ screening of plants targeted for improved biofuels production (1, 2, 20). Our ElectroNeedle technology is a unique combination of photodefinable Foturan glass to fabricate individually addressable microneedles through diazonium electrodeposi-

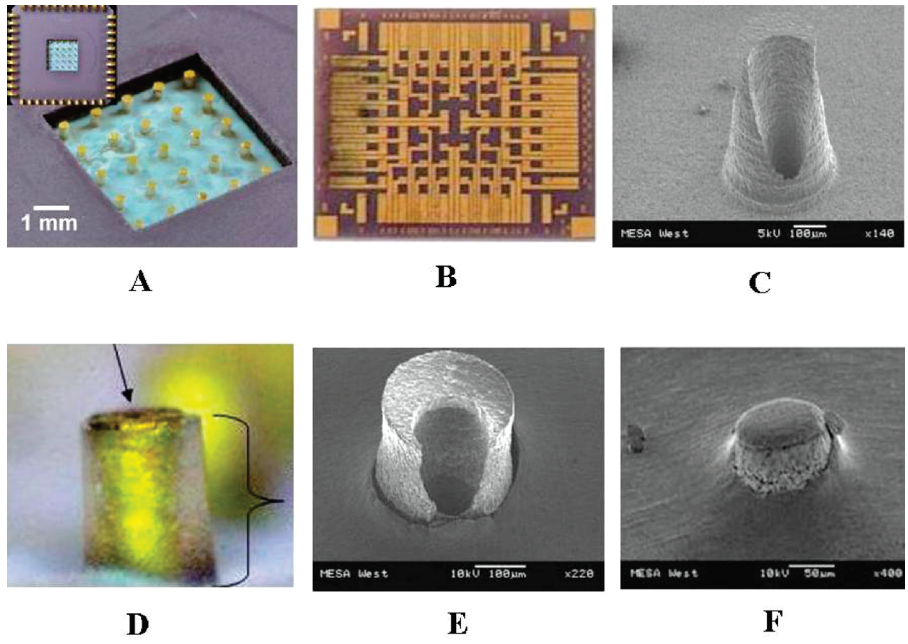

FIGURE 2. Examples of ElectroNeedle devices: (A) 1 cm^2, 5 × 5 array of individually addressable ElectroNeedles; (B) backside electrical contacts; (C) an individual hollow microneedle fabricated with Foturan; (D) single ElectroNeedle (400−500 μm tall with outer and inner diameters of approximately 250 and 100 μm, respectively) showing the protective dielectric sheath (indicated by the bracket), leaving the electrode exposed at the tip (indicated by a downward-pointing arrow); (E) Foturan microneedle piercing a 125-μm-thick aluminum foil without damage to the needle; (F) Foturan microneedle piercing 25-μm-thick steel. Parts C, E, and F are SEM images; the remaining parts are optical microscopic images.

tion chemistry (5–7), along with exposed electrodes and penetrable needles, to enable the minimally invasive piercing of micrometer-thick surfaces such as plant leaves, petals, or stems (8, 9). An integrated, miniaturized, high-throughput, field-deployable, point-of-test system such as the ElectroNeedles sensor array might facilitate real-time, on-site, and in situ analyses of biofuel-related biochemicals instead of a conventional role in drug delivery (3).

Foturan® Microfabrication. A unique feature of our microfabrication was the choice of material, Foturan, a directly photopatternable glass, which, when exposed to UV light and heated, generates ceramic crystallites that are 20−30 times more soluble in HF than the surrounding vitreous regions of unexposed glass (22). Furthermore, the experimental evidence was that we could fabricate parts with glass that had through-holes with no detectable degradation to the unexposed regions of the glass. The greater susceptibility to HF allowed the preferential anisotropic etching, which was sufficient to achieve a high aspect ratio (hole depth-to-width). Excellent aspect ratios have been reported using Foturan (26). ElectroNeedle arrays were produced using standard semiconductor processes of microfabrication techniques: photolithography, etching, and thin film deposition.

Microneedle Properties. The needles were constructed in two arrays of independently addressable electrodes: 5 × 5 and 10 × 10 (25 and 100 independently addressable microneedles, respectively; Figure 2A,B). The geometry of the needles and parameters such as the height, diameter, and needle density in the arrays are adjustable during microfabrication, affording manufacturing flexibility. We controlled the via sidewall shape by varying the aspect ratio (height to width or elevation to recess), the UV source during exposure, as well as etching from one or both sides of the wafer. The needles were 400−500 μm tall, and the outer and inner diameters were approximately 250 and 100 μm (Figure 2C,D). The needles have a sheath (Figure 2D) that protected the gold from buckling or deformation under the insertion force. The microneedles are sharp, long, and rugged for insertion into plant leaves, petals, or stems without bending or breaking, as evidenced by their ability to pierce 125-μm-thick aluminum (Figure 2E) or 25-μm-thick steel (Figure 2F). Furthermore, microneedles were not broken or deformed during repeated punctures of the aluminum. Because the metal microneedle passes fully through the glass substrate, individual electrical connections were made to each microneedle from the back of the substrate (Figure 2B) and thus did not interfere with the sensor needle tip (Figure 2D). A Foturan wafer with ten 10 × 10 ElectroNeedle arrays and a single packaged array are shown in Figure 3A,B.

Microfabrication Benefits and Caveats. Because our devices are made from glass, they have no boundary regions with varying chemical, mechanical, or optical properties. Microfabrication required only a UV light source, an oven, and chemical baths for equipment. Fabrication time scales were 2−3 days, facilitating rapid development of newer designs or optimizing existing steps. Operator intervention was limited to less than half a day. Our microfabrication permits the rapid production of strong, robust, durable, low-cost microneedle devices by batch manufacturing compared to the conventional Bosch processing (4). The glass used is biocompatible (28) and therefore suitable for biological applications. The combination of penetrable needles

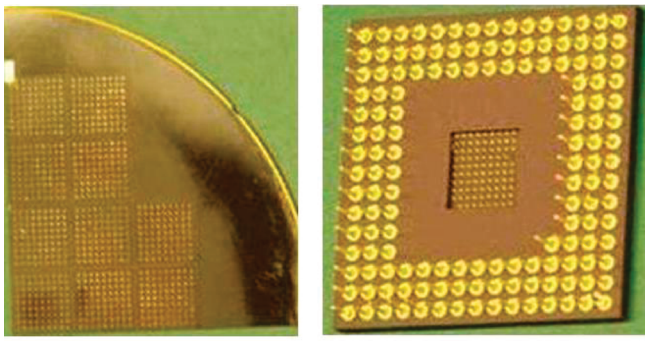

FIGURE 3. Examples of microfabricated ElectroNeedles: (A) ten 10 × 10 arrays; (B) a single, packaged 10 × 10 array.

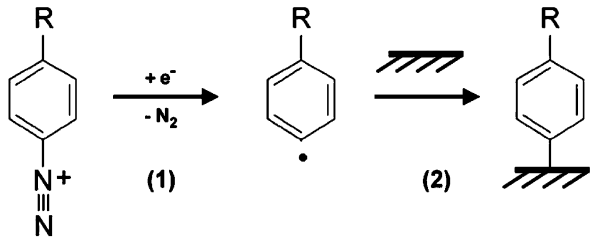

FIGURE 4. Mechanism of diazonium assembly onto metal, semiconductor, and electrode surfaces. (1) Electroreduction of the diazonium yields a phenyl-centered radical followed by (2) covalent bond formation between the radical and the conducting or semiconducting substrate.

and exposed electrodes permits minimally invasive, on-site, in situ biochemical measurements on micrometer-thick plant surfaces for biofuel analytes.

The rate-limiting step is the bake cycle that lasts up to 8 h. Certain process steps such as the UV intensity, exposure, and etch times are variable depending upon the particular batch of Foturan wafers, its pretreatment, and aging of the wafers prior to microfabrication. Other factors influencing our microfabrication included the critical role of polishing before bonding in order to achieve uniform plating across the wafer and ensuring the wetting of the vias prior to plating. As a parallel path, a liquid metal matrix fill and sintering for via fill might be considered.

Diazonium Chemistry. Phenyl films with various functional groups were covalently linked to the gold surface by the electroreduction of diazonium salts, as described in the Materials and Methods section titled "Electrode Modification and *p*-Cresol Measurements." This chemistry permitted the sensitive detection of *p*-cresol at individually addressable electrodes. The electrochemical reduction of a diazonium salt creates an aryl radical after spontaneous elimination of N_2 (Figure 4). The aryl radicals then form a covalent bond with conducting and semiconducting surfaces. The resulting film is highly stable and withstands several minutes of ultrasonication and long-term storage exposed to air while remaining conductive and thus facilitating subsequent electrochemistry. The functional groups on the electrode surface introduced by phenyl diazonium deposition may also enhance the interaction of the electrode with *p*-cresol, leading to higher currents and improving the sensitivity of detection.

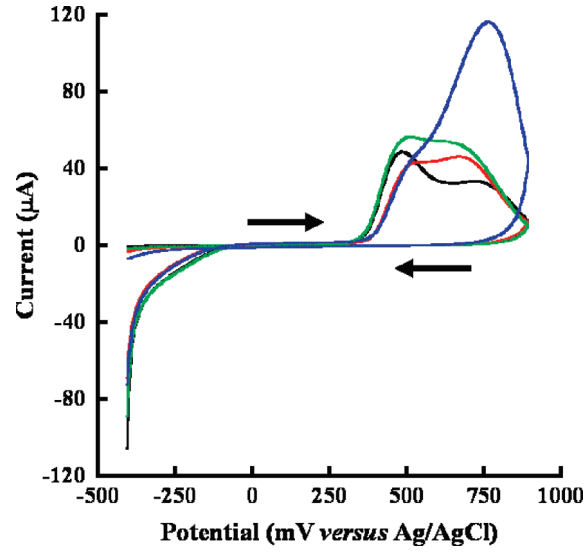

FIGURE 5. Cyclic voltammograms showing *p*-cresol oxidation at variously modified 5-mm-diameter gold electrode surfaces. The tracings with the unmodified and variously modified gold electrodes are as follows: unmodified (black); nitrophenyl thin film (red); carboxylphenyl thin film (green); aminophenyl thin film (blue). *p*-Cresol (5 mM) in a 50 mM sodium phosphate buffer, pH 7.4, was scanned at 100 mV/s. The arrows indicate the potential scanning directions.

Electrochemistry of *p*-Cresol. *p*-Cresol is a phenolic substrate for laccase (11), an enzyme implicated in lignin engineering and degradation (10). In the Introduction section of the paper, we outlined several reasons behind our interest in *p*-cresol, chiefly because of the molecule's role in lignin degradation and thus enabling second-generation biofuels (1). We, therefore, chose *p*-cresol for electrochemical assays using ElectroNeedles, in order to demonstrate its relevance to biofuel applications. Electrochemical detection of *p*-cresol was optimized using disposable 5-mm-diameter gold disk electrodes (Figure 5) before transferring the assay to ElectroNeedles, thus preserving the latter for the sensitive detection of the analyte.

Oxidation of *p*-cresol on a bare gold surface showed two oxidative waves near +500 and +735 mV versus Ag/AgCl, similar to previous reports of *p*-cresol detection on glassy carbon electrodes (24). Oxidation of *p*-cresol on the nitrophenyl-modified gold surface showed a slightly reduced and positively shifted initial peak at +530 mV, followed by an enhanced and negatively shifted peak at +710 mV. The carboxylphenyl-modified gold surface showed *p*-cresol oxidation currents at +510 and +660 mV, higher than the bare and nitrophenyl-modified gold surfaces (Figure 5). *p*-Cresol electrochemistry on the aminophenyl-modified gold surface resulted in an initial oxidative peak nearly identical with the peak from the nitophenyl-modified gold surface. However, the second oxidative wave at +770 mV showed significantly enhanced currents, more than twice the signal obtained from the other surfaces (Figure 5). The differences in the acid–base pairing between the varying phenyl surfaces and *p*-cresol might result in variation of the complementary π-donor–acceptor interactions, leading to the observed differences in the peak potentials and currents.

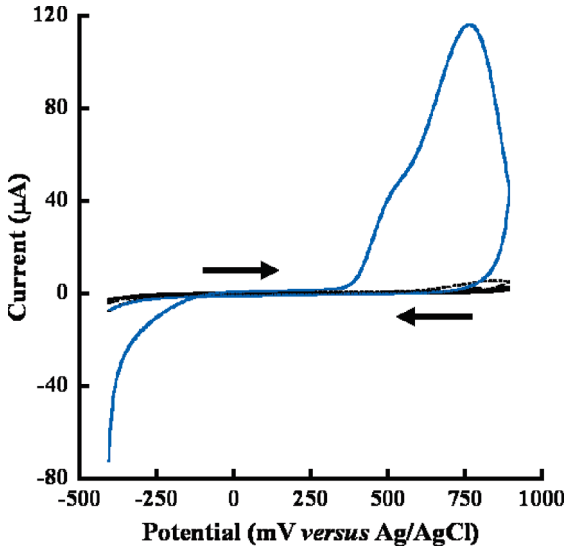

FIGURE 6. Sequential cyclic voltammograms of an aminophenyl-thin-film-modified, 5-mm-diameter gold electrode. *p*-Cresol (5 mM) in a 50 mM sodium phosphate buffer, pH 7.4, was scanned at 100 mV/s. Except for the first scan cycle (blue tracing), the remaining four scans (black tracings) showed significantly reduced currents over the entire potential range. The arrows indicate the potential scanning directions.

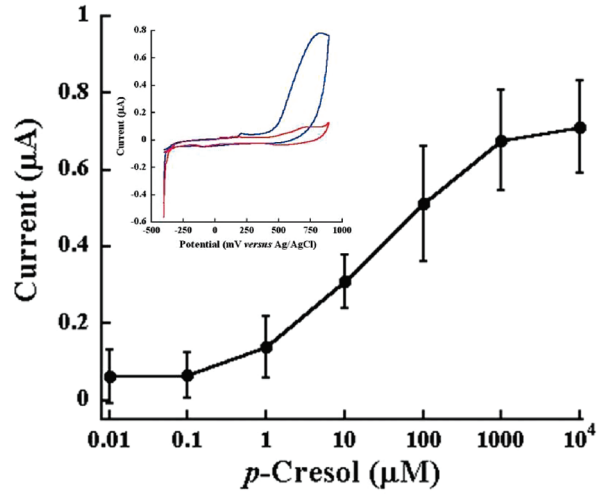

FIGURE 7. *p*-Cresol detection at aminophenyl-thin-film-modified gold ElectroNeedles (250-μm outer diameter). Oxidative currents were obtained at +770 mV versus Ag/AgCl from CV in a 50 mM sodium phosphate buffer solution, pH 7.4; the scan rate was 100 mV/s. Error bars represent the standard deviation values obtained from measurements at three or more individually addressable ElectroNeedle posts. The inset shows a representative CV obtained at an ElectroNeedle post in a 5 mM *p*-cresol solution (blue trace). Also included in the inset is the background CV measurement (a sodium phosphate buffer solution without *p*-cresol) obtained prior to the *p*-cresol measurement at the same ElectroNeedle post (red trace).

Initially, 5-mm-diameter phenylamine-coated gold electrodes were used for estimation of the *p*-cresol sensitivity. Because of radical formation and fouling of the working electrode surface (24), each electrode was used only for a single measurement. Background measurements were taken using a 50 mM sodium phosphate buffer (without *p*-cresol), followed by measurements of 1 mM, 500 μM, 100 μM, 10 μM, 1 μM, and 1 nM *p*-cresol. The current response obtained at +770 mV over concentrations of 1 mM to 100 nM showed that the electrochemical assay was quantitative with a detection limit in the high nanomolar range.

We next determined whether the phenyl-modified gold surfaces could resist passivation by performing five sequential CV scans in a *p*-cresol solution. The product of *p*-cresol oxidation is a highly reactive phenoxy radical species that polymerizes in solution near the electrode surface (24). This resulted in a passivating layer on the electrode within seconds and thereby significantly reduced the current response of the electrode. All of the surfaces prepared in this study were subject to passivation/fouling because diminished currents without any detectable oxidative waves were obtained for scans 2−5 (Figure 6). Following the first scan on an aminophenyl surface, currents decreased from 116 to 4 μA and did not recover even after thorough rinsing of the electrode with 18 MΩ·cm water and repeating of the electrochemical assay using a fresh *p*-cresol solution. It was concluded that the simple phenyl thin film became fouled because of passivation as described above.

p-Cresol Detection Using ElectroNeedles. Enzymes such as laccase and/or tyrosinase were used to metabolize *p*-cresol into a more electrochemically reversible analyte, thereby minimizing the passivation/fouling effects. Thus, enzyme-immobilized electrodes permitted reuse of the detector (29). For example, laccase might be immobilized upon the microneedle surface using the protocols described previously (7, 30). However, functionalization of ElectroNeedles with enzymes was not pursued because maintaining the activity of the immobilized enzyme over the long term complicated the sensor design. These experiments will be a part of our future efforts with the ElectroNeedles. The ElectroNeedle technology platform was designed here as a point-of-test tool for biofuel analytes. In such a situation, a single-use, disposable array should be adequate.

Fabricated solid post ElectroNeedle devices (Figures 2 and 3) were used next to detect and quantize *p*-cresol. Aminophenyl thin films were electrodeposited onto the gold ElectroNeedles, similar to the procedures used for the disposable 5-mm gold disk electrodes (above). Electrochemical measurements of *p*-cresol concentrations were randomized and performed at a minimum in triplicate (Figure 7). Each of the 25 ElectroNeedle posts in the 5 × 5 array was used only once because *p*-cresol oxidation led to electrode fouling (24), although to a lesser extent than that observed for the 5-mm gold disk electrodes. Two CV scans were performed in *p*-cresol solutions at each ElectroNeedle post. The second scan yielded oxidative currents that were 48 ± 16% of the first *p*-cresol oxidative current. This is compared to the less than 5% oxidative current obtained from second CV scans at 5-mm gold disk electrodes. This may be due to a more radial diffusion profile at the much smaller diameter of the ElectroNeedles, leading to faster diffusion of the phenoxy radicals away from the electrode surface. The oxidative detection currents were linear over 3 orders of magnitude of *p*-cresol concentrations (1 μM to 1 mM). Concentrations greater than 1 mM lead to a saturated current response (Figure 7). The *p*-cresol LOD and LOQ using

Table 1. LODs and LOQs of *p*-Cresol

		fluorescence	
assay metric	electrochemical value	$\lambda_{ex} = 262$ nm[a]	$\lambda_{ex} = 322$ nm[a]
LOD (μM)	1.8	0.8	0.4
LOQ (μM)	16.0	25.0	3.0
LOD (ppb)	194	87	43
LOQ (ppb)	1724	2700	324
r^2	0.9798[b]	0.99851[c]	0.99932[c]

[a] For the fluorescence assays, LOD and LOQ values were calculated from reactions of 5 ng/μL laccase-catalyzed *p*-cresol oxidation. Fluorescence emission was measured at 425 nm as described previously (11). [b] Derived from a logarithmic curve fit of the data between 0.1 and 1000 μM *p*-cresol. [c] Correlation of coefficient values were determined using a linear curve fit of the 5 ng/μL laccase dose–response curve.

the ElectroNeedles were 1.8 and 16 μM, respectively (Table 1). Our data are in agreement with the micromolar concentrations of *p*-cresol detected previously using tyrosinase-immobilized electrodes (29) and superior to the 0.25–4 mM *p*-cresol calibration reported recently using zeolite-coated electrodes (31). A distinguishing characteristic of the ElectroNeedle technology is its throughput capability. Using 5 × 5 or 10 × 10 arrays, the ElectroNeedles have the capability of analyzing 25 or 100 different analytes simultaneously or executing 25 or 100 independent measurements of a single analyte for statistical rigor. Another application might be phytochemical profiling in various regions over the thin surfaces of a petal, leaf, or stem.

Fluorescent Assay for *p*-Cresol. Electrochemical assays have made significant progress over the past decades, with several assays reporting detection limits that rival those of fluorescence assays (32). Electrochemical detection is particularly promising for portable sensing because of its low power requirements, fast analysis times, and amenability to miniaturization by leveraging integrated circuit technology. Fluorescence spectroscopy, however, is the gold standard, especially because of sensitivity at the single-molecule level (33). We, therefore, validated the ElectroNeedles system performance against a fluorescent assay for *p*-cresol based upon laccase oxidation (11). As predicted previously, we improved the sensitivity of *p*-cresol detection by greater than 10-fold through changes in the laccase and *p*-cresol concentrations along with the catalysis time (Figure 8a,b). The LOD of 0.4 μM was less than 1 order of magnitude more sensitive than electrochemical detection (Table 1). With the suboptimal excitation wavelength of 262 nm (11), the LOD of 0.8 μM *p*-cresol was approximately 2-fold better than electrochemical detection (Table 1).

Nevertheless, the electrochemical assay for *p*-cresol nearly rivaled the sensitivity of the fluorescence system, even though the latter benefitted from laccase-catalyzed enhancement. It should be noted that the electrochemical assay was considerably faster, requiring less than 2 min to complete a CV sweep. This is in contrast to the 60 min of laccase catalysis (Figure 8), followed by fluorescence measurements. The fluorescence assay showed smaller errors between measurements (Figure 8a,b). Errors in the electrochemical assay may be minimized by improving ElectroNeedle fabrication in order to ensure a uniform electrode surface area between the microneedles.

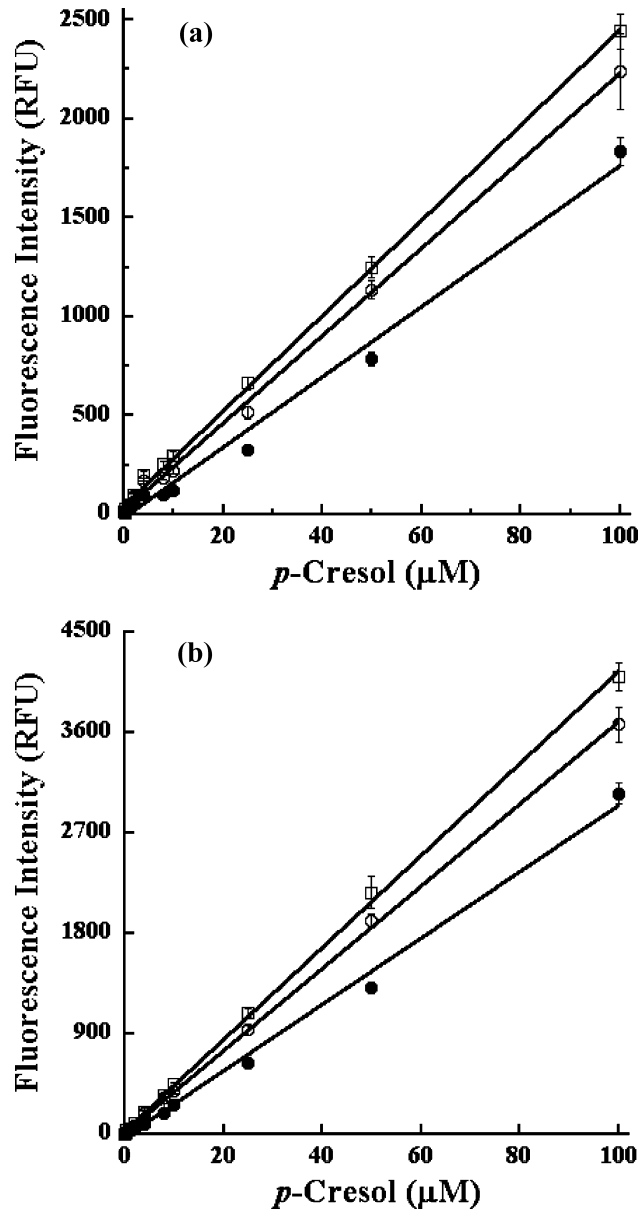

FIGURE 8. (a) *p*-Cresol calibration using a 262-nm excitation wavelength. Increasing concentrations of laccase-oxidized *p*-cresol were excited using 262-nm wavelength light, and the fluorescence emission was monitored at 425 nm. Dose–response curves were obtained by oxidation of *p*-cresol using 1 ng/μL (closed circles), 2.5 ng/μL (open circles), and 5 ng/μL (open squares) laccase enzymes. The linearity (correlation coefficient, r^2) values for the three tracings were 0.98931, 0.99812, and 0.99851, respectively. (b) *p*-Cresol calibration using a 322-nm excitation wavelength. Increasing concentrations of laccase-oxidized *p*-cresol were excited using 322-nm wavelength light, and the fluorescence emission was monitored at 425 nm. Dose–response curves were obtained by oxidation of *p*-cresol using 1 ng/μL (closed circles), 2.5 ng/μL (open circles), and 5 ng/μL (open squares) laccase enzymes. The linearity (correlation coefficient, r^2) values for the three tracings were 0.99486, 0.99958, and 0.99932, respectively.

CONCLUDING REMARKS

The combination of individually addressable ElectroNeedles through diazonium electrodeposition (Figure 4) along

with the exposed electrodes and penetrable needles (Figure 2), confers minimally invasive, high-throughput, multiplexed, point-of-test capabilities and facilitates in situ measurements of biofuel-related biochemicals. In a departure from the past drug-delivery work using microneedles, we describe the sensor capabilities of our ElectroNeedles. The performance of ElectroNeedles was comparable to the gold standard fluorescence detection. Our future efforts will report the field performance of the ElectroNeedles technology platform by testing penetrable plant surfaces such as stems, leaves, and petals (8, 9).

Acknowledgment. The DOE's JBEI (http://www.jbei.org) is supported by the U.S. Department of Energy, Office of Science, Office of Biological and Environmental Research, through Contract DE-AC02-05CH11231 between Lawrence Berkeley National Laboratory and the U.S. Department of Energy. Sandia is a multiprogram laboratory operated by Sandia Corp., a Lockheed Martin Company, for the United States Department of Energy under Contract DE-AC04-94AL85000. These investigations were partially funded by Sandia's Laboratory Directed Research and Development (LDRD) Project 125859 and by the Defense Threat Reduction Agency, Joint Science and Technology Office (DTRA-JSTO), Project MIPR9FO89XR052-0, both awarded to K.A. We thank Drs. Christopher Apblett, Edwin Heller, Stanley Kravitz, David Ingersoll, Stephen Casalnuovo, and Kent Schubert for microfabrication project support. Carrie Schmidt and Michael Thomas provided technical assistance.

REFERENCES AND NOTES

(1) Simmons, B. A.; Loque, D.; Blanch, H. W. *Genome Biol.* **2008**, *9*, 242.1−242.6.
(2) Blanch, H. W.; Adams, P. D.; Andrews-Cramer, K. M.; Frommer, W. B.; Simmons, B. A.; Keasling, J. D. *ACS Chem. Biol.* **2008**, *3*, 17–20.
(3) Vandervoort, J.; Ludwig, A. *Front. Biosci.* **2008**, *13*, 1711–1715.
(4) Roxhed, N.; Griss, P.; Stemme, G. *J. Micromech. Microeng.* **2007**, *17*, 1087–1092.
(5) Delmar, M.; Hitmi, R.; Pinson, J.; Saveant, J. M. *J. Am. Chem. Soc.* **1992**, *114*, 5883–5884.
(6) Harper, J. C.; Polsky, R.; Dirk, S. M.; Wheeler, D. R.; Brozik, S. M. *Electroanalysis* **2007**, *19*, 1268–1274.
(7) Polsky, R.; Harper, J. C.; Wheeler, D. R.; Dirk, S. M.; Arango, D. C.; Brozik, S. M. *Electroanalysis* **2008**, *20*, 671–679.
(8) Vile, D.; Garnier, E.; Shipley, B.; Laurent, G.; Navas, M.-L.; Roumet, C.; Lavord, S.; Diaz, S.; Hodgson, J. G.; Lloret, F.; Midgley, G. F.; Poorter, H.; Rutherford, M. C.; Wilson, P. J.; Wright, I. J. *Ann. Botany* **2005**, *96*, 1129–1136.
(9) Chandran, S.; Toh, C. L.; Zuliana, R.; Yip, Y. K.; Nair, H.; Boyce, A. N. *J. Appl. Horticulture* **2006**, *8*, 117–120.
(10) Riva, S. *Trends Biotechnol.* **2006**, *24*, 219–226.
(11) Achyuthan, K. E.; McClain, J. L.; Raj, D. *Comb. Chem. High Throughput Screening* **2009**, in press.
(12) Peters, F.; Heintz, D.; Johannes, J.; van Dorsselaer, A.; Boll, M. *J. Bacteriol.* **2007**, *189*, 4729–4738.
(13) Leonowicz, A.; Cho, N.-S.; Luterek, J.; Wilkolazka, A.; Wojtas-Wasilewska, M.; Matuszewska, A.; Hofrichter, M.; Wesenberg, D.; Rogalski, J. *J. Basic Microbiol.* **2001**, *41*, 185–227.
(14) Klein, M. T.; Virk, P. S. *Energy Fuels* **2008**, *22*, 2175–2182.
(15) Hassan, E. M.; Steele, P. H.; Ingram, L. *Appl. Biochem. Biotechnol.* **2009**, *154*, 182–192.
(16) Xia, Z.; Yoshida, T.; Funaoka, M. *Eur. Polym. J.* **2003**, *39*, 909–914.
(17) Okuda, K.; Ohara, S.; Umetsu, M.; Takami, S.; Adschiri, T. *Bioresour. Technol.* **2008**, *99*, 1846–1852.
(18) Wariishi, H.; Dunford, H. B.; MacDonald, I. D.; Gold, M. H. *J. Biol. Chem.* **1989**, *264*, 3335–3340.
(19) Hynd, B. *Methods in Molecular Biology, volume 190, High Throughput Screening: Methods and Protocols*; Janzen, W. P., Ed.; Humana Press Inc.: Totowa, NJ, 2002; Vol. 190, pp 229−243.
(20) Sticklen, M. B. *Nat. Rev. Genet.* **2008**, *9*, 433–443.
(21) McNab, H.; Monahan, L. C. *J. Chem. Soc., Perkin Trans.* **1989**, *3*, 419–424.
(22) Dietrich, T. R.; Ehrfeld, W.; Lacher, M.; Kraemer, M.; Speit, B. *Microelectron. Eng.* **1996**, *30*, 497–504.
(23) Kreibig, U. *Appl. Phys.* **1976**, *10*, 255–264.
(24) Wang, J.; Martinez, T.; Yaniv, D. R.; McCormick, L. D. *J. Electroanal. Chem.* **1991**, *313*, 129–140.
(25) Rajaraman, R.; Henderson, H. T. *Sens. Actuators, B* **2005**, *105*, 443–448.
(26) Kim, K.; Lee, J.-B. *Microsyst. Technol.* **2007**, *13*, 231–235.
(27) Cheng, Y.; Sugioka, K.; Midorikawa, K. *Opt. Exp.* **2005**, *13*, 7225–7232.
(28) Kim, J.; Berberoglu, H.; Xu, X. J. *Microlith. Microfab. Microsyst.* **2004**, *3*, 478–485.
(29) Rogers, K. R.; Becker, J. Y.; Cembrano, J. *Electrochim. Acta* **2000**, *45*, 4373–4379.
(30) Gill, H. S.; Prausnitz, M. R. *Pharm. Res.* **2007**, *24*, 1369–1380.
(31) Berge-Lefranc, D.; Eyraud, M.; Schaf, O. *C. R. Chim* **2008**, *11*, 1063–1073.
(32) Schwarz, M. A.; Hauser, P. C. *Lab Chip* **2001**, *1*, 1–6.
(33) Moerner, W. E.; Fromm, D. P. *Rev. Sci. Instrum.* **2003**, *74*, 3597–3619.

AM900259U